

Graphical Abstract

AI-Assisted Object Condensation Clustering for Calorimeter Shower Reconstruction at CLAS12

Gregory Matousek, Anselm Vossen

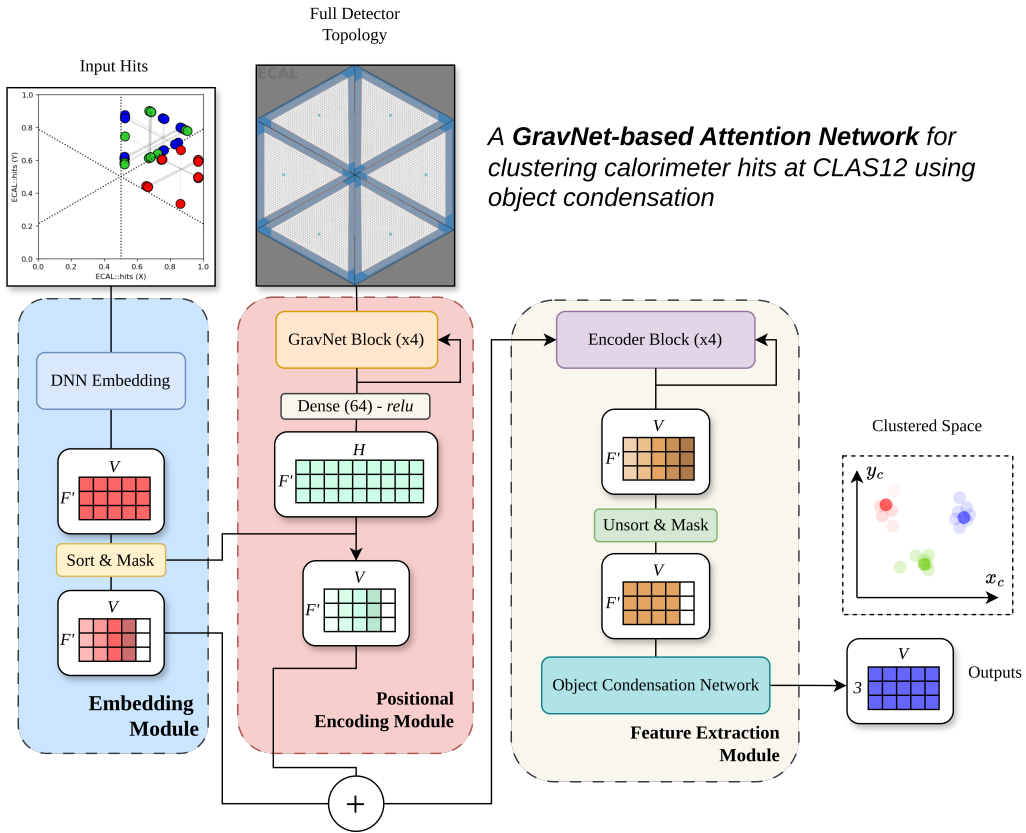


Figure 1: Schematic of clustering network architecture.

Highlights

AI-Assisted Object Condensation Clustering for Calorimeter Shower Reconstruction at CLAS12

Gregory Matousek, Anselm Vossen

- Introduces an AI-based clustering method for CLAS12's electromagnetic calorimeter.
- Uses GravNet and a Transformer encoder to learn hit representations.
- Implements object condensation as a framework to perform hit clustering.
- First AI clustering method applied to hodoscopic detectors.

AI-Assisted Object Condensation Clustering for Calorimeter Shower Reconstruction at CLAS12

Gregory Matousek^{a,*}, Anselm Vossen^b

^a*Duke University, 120 Science Drive, Durham, 27708, NC, USA*

^b*Thomas Jefferson National Accelerator Facility, 12000 Jefferson Avenue, Newport News, 23606, VA, USA*

Abstract

Several nuclear physics studies using the CLAS12 detector rely on the accurate reconstruction of neutrons and photons from its forward angle calorimeter system. These studies often place restrictive cuts when measuring neutral particles due to an overabundance of false clusters created by the existing calorimeter reconstruction software. In this work, we present a new AI approach to clustering CLAS12 calorimeter hits based on the object condensation framework. The model learns a latent representation of the full detector topology using GravNet layers, serving as the positional encoding for an event's calorimeter hits which are processed by a Transformer encoder. This unique structure allows the model to contextualize local and long range information, improving its performance. Evaluated on one million simulated $e + p$ collision events, our method significantly improves cluster trustworthiness: the fraction of reliable neutron clusters, increasing from 8.98% to 30.65%, and photon clusters, increasing from 51.10% to 63.64%. Our study also marks the first application of AI clustering techniques for hodoscopic detectors, showing potential for usage in many other experiments.

Keywords: particle physics, calorimeters, machine learning, clustering, self-attention, object condensation

*Corresponding author. *E-mail address:* gregory.matousek@duke.edu

1. Introduction

The CLAS12 detector system at Jefferson Lab, Virginia, measures high energy collisions of electrons and nucleons to advance our understanding of fundamental nuclear physics. These collisions produce particles that travel through and interact with the experiment’s detectors. Similar to many other particle physics experiments, CLAS12 uses detectors called electromagnetic calorimeters (ECals) [1] to help measure the type, position and energy of these final state particles.

The CLAS12 ECal is important for measuring photons and neutrons. These particles do not leave tracks in the tracking detectors and can therefore only be identified using their energy deposits in the calorimeters. Physics studies using photons from π^0 decays or neutrons from exclusive events thus rely on the ECal for accurate reconstruction of these particles. Inefficiencies in the collaboration’s analysis pipeline COATJAVA lead to an overabundance of *fake* neutral particles being reconstructed (shown in Figure 2), complicating these studies.

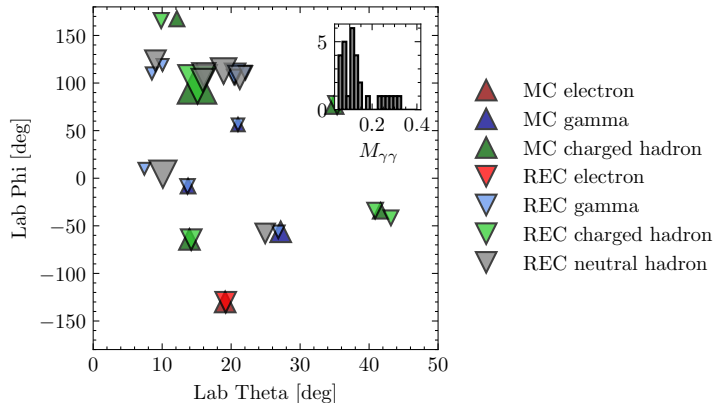


Figure 2: Sample $e + p$ Monte Carlo event at CLAS12 reconstructed using COATJAVA plotted in (θ, ϕ) space. Upwards (downwards) facing triangles represent the final state true (reconstructed) particles. Marker size roughly scales with particle energy. In the top right subplot, the invariant mass distribution of all reconstructed $\gamma\gamma$ pairs in the event is shown. Many excess photon and neutrons are reconstructed, despite there being only three true photons in the event.

In this work, we propose an AI model that significantly enhances the clustering accuracy of ECal hits at CLAS12. The network learns hit positional encodings using a module composed of consecutive GravNet layers [2] which

process the complete ECal detector topology. The learned encodings are combined with the embedded hit representations for each event, and the resulting feature vector is then processed by a Transformer encoder [3]. Then, a multi-layer perceptron (MLP) network clusters tokens (hits) belonging to the same particle by mapping them to similar regions in an 2-dimensional latent space. This clustering strategy, known as object condensation (OC), was first introduced in Ref. [4] and has since been employed in several nuclear and particle physics AI clustering methods [5, 6]. To our knowledge, this work represents the first instance of AI-assisted clustering applied to hodoscopic detectors. Another novelty is that the network combines fine-grained local neighborhood representations (GravNet) with long range contextual information (self-attention) to strengthen event reconstruction.

The paper is organized as follows: Section 2 gives an overview of machine learning applications in particle and nuclear physics, with a focus on clustering tasks. Section 3 describes the CLAS12 electromagnetic calorimeter and the current COATJAVA clustering method. In Section 4, we describe the event simulation and dataset. Section 5 showcases the new model architecture for performing ECal hit clustering, and discusses the object condensation loss. In Section 6, the results of the model are shown, and a new metric is defined to compare with COATJAVA . We summarize our findings and detail future work in Section 7.

2. Related Work

Machine learning applications in particle and nuclear physics are constantly evolving, with tasks ranging from clustering, identification, regression, and fast simulation. A living review containing hundreds of these applications can be found in Ref. [7]. Graph neural network (GNN) based architectures form the backbone of the majority of detector-based clustering tasks. This is due to their ability to represent irregular detector topologies with a flexible learned latent representation [8, 9]. We separate this discussion to remark on the current progress of AI approaches to track and calorimeter clustering.

2.1. Track clustering

The Exa.TrkX collaboration’s **GNN4ITk** [10] pipeline performs track clustering by first constructing a graph where nodes represent hits in the silicon inner tracker. The GNN edges are scored to assign low/high probability

connections. After edge filtering, track candidates are collected in an iterative graph segmentation stage. GNN4ITk’s edge classification framework became a leading approach, inspiring further improvements and models for addressing the high multiplicity challenges of the future HL-LHC.

Hierarchical Graph Neural Networks **HGNNs** [11] addresses the difficulty of handling disconnected tracks with GNN track clustering. Initial connectivity during graph construction may prohibit a disconnected track from being properly reconstructed. In HGNN, track segments are pooled into *super-nodes*, at which a k-NN operating on super-nodes allows message passing between broken segments, increasing the receptive field and preserving long-range relationships. This in turn allows the model to learn to combine disconnected track segments to form one track.

The LHCb collaboration’s **ETX4VELO** [12] model builds on GNN4ITk, addressing another major concern with GNN track clustering — node sharing tracks. Identifying two tracks tending to the same shared node(s) is solved by introducing an additional classifier that operates on a graph of the edges. In a *triplet-building* stage, the model learns to duplicate nodes belonging to separate tracks, splitting the network into multiple tracks, making clustering more straightforward.

The Evolving Graph-based Graph Attention Network **EggNet** [6] avoids explicit initial graph construction by allowing the nodes to learn edges connections dynamically. When the final edge connections are proposed, each contributes some amount to an object condensation based loss term based on if the two connected nodes belong to the same particle. This approach enhances message passing, improves graph efficiency, and mitigates issues related to missing track connections.

Transformer-based models use more modern architectures compared with traditional GNN methods. One such model [13] uses the **MaskFormer** architecture — originally developed for image segmentation [14] — to simultaneously assign hits to tracks and predict track properties. The approach begins with a Transformer encoder with a sliding window to filter hits by classifying them as signal or noise. The signal hits are then processed through a fixed-window encoder-decoder module that generates multiple binary masks corresponding to hit-to-track assignments. The model was tested on the TrackML dataset with great success and shows a growing trend for integrating computer vision-inspired solutions to clustering.

2.2. Calorimeter clustering

A **fuzzy-clustering GNN** [9] was developed for the Belle II experiment to address overlapping photon showers from π^0 decays in their electromagnetic calorimeter. In this work, each calorimeter crystal performs message-passing in a dynamically generated graph using GravNet [2]. The GNN predicts a set of weights that determine the fractional assignment of each hit to multiple potential clusters, allowing for partial energy contributions to overlapping photon showers. The study outperforms the baseline Belle II reconstruction algorithm, achieving a 30% improvement in energy resolution for the low energy photons in asymmetric photon pairs.

An **object condensation-based GravNet** approach [15] was developed for the CMS High Granularity Calorimeter (HGCal) at the future HL-LHC, where up to 200 simultaneous proton-proton interactions may occur. Similar to Belle II, due to the irregular geometry of the HGCal, GravNet’s flexibility in assigning nearest neighbors allows for efficient clustering. For each hit, the network predicts object condensation variables for clustering, as well as cluster properties such as particle energy. This study demonstrates the potential for end-to-end multi particle reconstruction at the HL-LHC.

3. The CLAS12 Electromagnetic Calorimeter

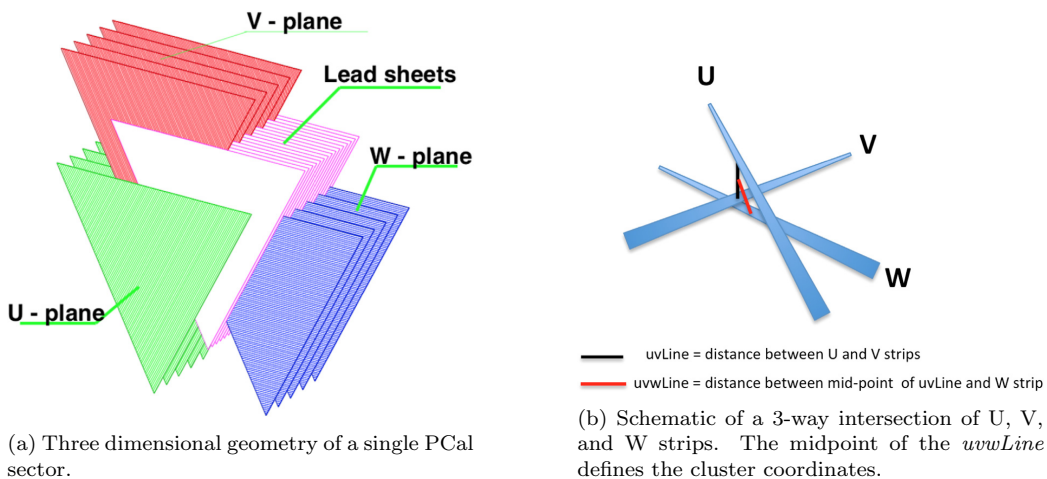


Figure 3: View of the U, V, W scintillating strip plane layout at CLAS12 [16].

CLAS12’s forward detector system consists of 6 distinct azimuthal sectors arranged around the beam pipe. The z-axis is defined in the laboratory frame

in the direction of the electron beam. The x-axis points horizontally and the y-axis points upwards. Each sector contains three calorimeter subsystems, named the pre-shower calorimeter (PCal), inner calorimeter (ECin) and the outer calorimeter (ECout), ordered in increasing distance from the collision point. Each subsystem is a sampling calorimeter comprised of 1cm thick scintillator strips and 1/4cm thick lead sheets [16] (see Figure 3a). Each of the six sectors' PCal contains 192 scintillator strips, the ECin 108 strips, and the ECout 108 strips, for a total of 2448 for the whole system. Scintillator strips are arranged in a triangular layout such that each layer of strips (named U, V, and W) are $\pm 120^\circ$ relative to one another.

Subatomic particles from the collision create secondary particles, primarily from interactions in the lead sheets. These secondaries emit light within the sensitive scintillator strips. The light generated in each strip is read out by photomultiplier tubes (PMTs) to record deposited energy. The individual reading of a strip in a collision event is referred as a *hit*. A *cluster* is a group of hits from the same initial particle.

Clusters are essential objects defined during event reconstruction that capture the position and total energy deposited by a particle. Collider experiments such as CMS [17], ATLAS [18], and ALICE [19] have grid-like calorimeter topologies and use a seeding algorithm to group hits into clusters. To form clusters at CLAS12, adjacent strips within the same layer (ex: U) are first collected into intermediate objects called *peaks*. In a process sketched in Figure 3b, COATJAVA determines a cluster using geometry by searching for 3-way intersections of U, V, W peaks. Besides CLAS12, ECals with hodoscopic geometries (ones that exploit cross-layered strips for determining cluster position using intersections) are seen in a range of physics experiments [20, 21, 22].

An important question to address is how does COATJAVA reconstruct *fake* neutral particles in the first place? For each cluster of ECal hits measured at CLAS12, COATJAVA looks for a track whose trajectory points towards the cluster centroid. Clusters without a matching track are classified as neutrals, and timing information, among other properties of the cluster, are used to distinguish between neutrons and photons. Fake neutral particles are most often reconstructed because COATJAVA incorrectly assigns multiple clusters that were in fact generated by one true particle. We see this happen in sample events such as one shown in Figure 4. In this event, the widely dispersed ECal hits from a single Monte Carlo neutron causes three separate neutral particles to be reconstructed. These reconstruction issues are able to

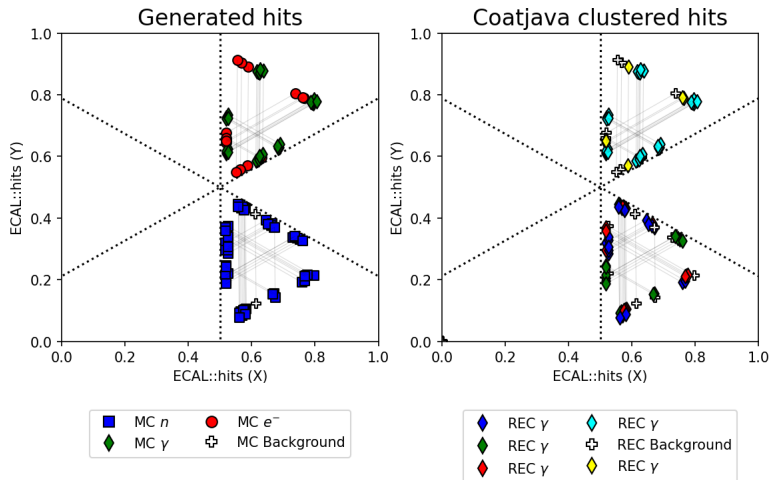


Figure 4: (Left) Simulated ECal detector response from multiple final state particles in a collision event. (Right) Clusters identified by the COATJAVA pipeline. In the bottom right sector, a true generated neutron deposits energy in many strips. From these strip hits, the clustering algorithm written in COATJAVA reconstructs three neutral particles.

be overcome through the design of our AI clustering model.

4. Dataset

In this work, one million $e+p$ fixed target Deep Inelastic Scattering (DIS) events (collisions) are generated using CLASDIS, a Semi-inclusive DIS (SIDIS) Monte Carlo based on PEPSI LUND [23]. The electron beam energy was set to 10.6 GeV to replicate the configuration of recent and ongoing CLAS12 experiments. Final state particles for each event are processed using a Geant4 Monte Carlo simulation framework called GEMC to create realistic detector readouts from CLAS12. For each event, the 150 ECal strips with the highest energy deposits are selected, and each is assigned 17 features—with zero-padding applied if fewer than 150 strips are hit. For each strip, the features are:

- The Cartesian coordinate endpoints for each strip, labeled x_o, y_o, z_o and x_e, y_e, z_e .
- The energy deposited in the strip.
- The timing recorded by the strip.

- 9 One-hot encoded bits to assign the strip’s layer number. There are 3 calorimeters (PCal, ECin, ECal) and a U,V,W layer for each.

All features, such as the timing information, are scaled between $[0, 1]$ to avoid exploding gradients during training.

An additional feature per strip, its STRIPID, uniquely identifies it among the 2448 strips in the CLAS12 ECal. The STRIPID is utilized in the model to cross-reference the strip coordinates and to match to correct positional encodings.

To properly train the clustering algorithm, hits belonging to the same particle in the event are assigned a unique true ID. To do so, the particle history of each ECal hit in an event is traced back in Geant4 to one of the final state particles generated in the collision. All zero-padded hits are assigned a true ID of -1 to mark them as background. In a pre-processing step, we check each sector’s PCAL, ECin, and ECal for at least one hit all three layers — U,V and W. If two or less are found, then those hits are considered background as later postprocessing steps require all three to form a cluster.

5. Methodology

5.1. Architecture

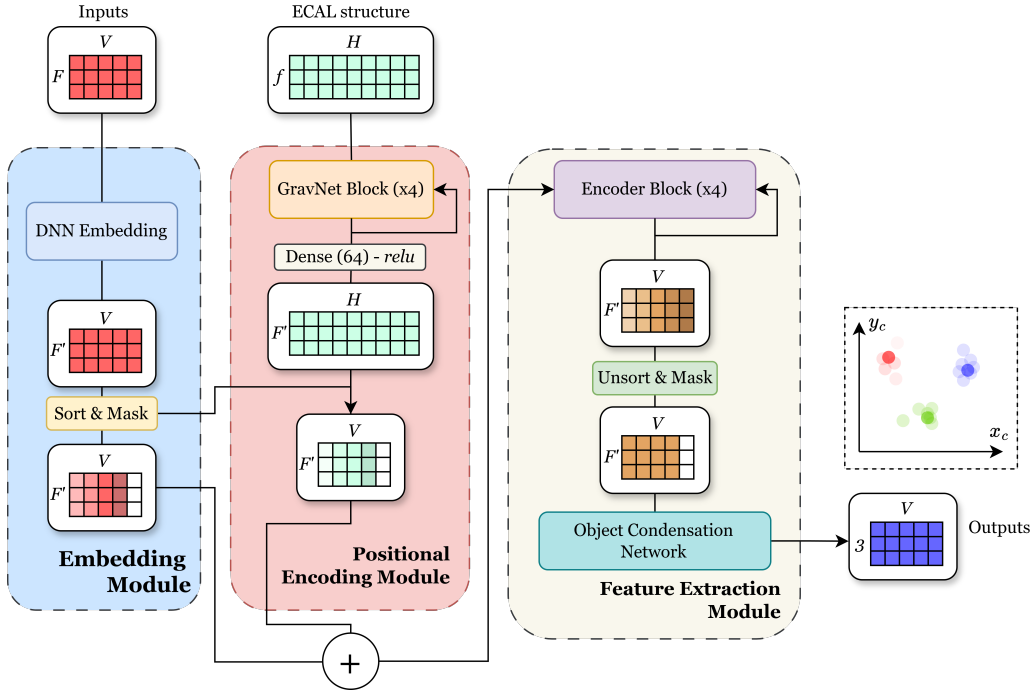
The model architecture is illustrated in Figure 5. The network is comprised of three modules — embedding, positional encoding, and feature extraction. The input is a point cloud $x \in \mathbb{R}^{V \times F}$ consisting of $V = 150$ ECal hits, where each point is represented by $F = 17$ features.

The point cloud x is passed through the embedding module f_{EMB} . Input node features are passed through a batch normalization layer and are then encoded using 3 MLPs with linear activations, followed by a 0.05 feature dropout (see Figure 5b). We then sort the output along the V -dimension by the STRIPID, saving the unmasked strip hits for the positional encoding. The output z of the embedding module is given by

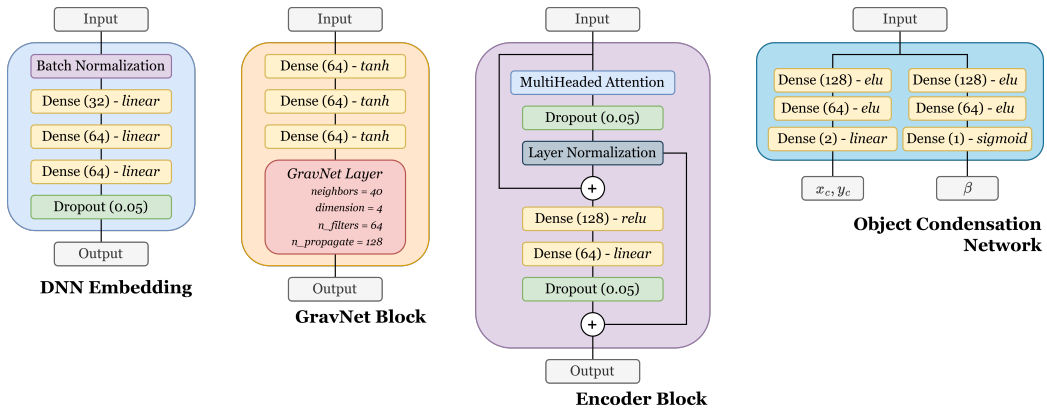
$$z \in \mathbb{R}^{V \times F'} = f_{\text{EMB}}(x), \tag{1}$$

where $F' = 64$.

At the same time, a positional encoding (PE) module f_{PE} receives as input $g \in \mathbb{R}^{H \times f}$ that represents the full detector topology. The $f = 6$ coordinate features representing each of the $H = 2448$ strips are the (x, y, z) of the two



(a) High-level view of the full architecture pipeline. Event-by-event ECal hits are inputted into the embedding module, preparing them for the encoder blocks. A positional encoding module trains on the entire detector topology, adding these encodings to the hits. A feature extraction module predicts object condensation variables for each hit for later clustering.



(b) Internal components of the networks modules. For this project, we utilize the Python library TensorFlow to construct each layer.

Figure 5: Schematic of the network architecture, highlighting: (a) the higher-level embedding, positional encoding, and feature extraction modules, (b) the sub-networks built into these modules.

strip endpoints. This fixed tensor is passed through 4 consecutive GravNet blocks, each containing 3 MLPs followed by a single GravNet layer.

Following the works of [9, 15], we chose GravNet [2] due to its ability to perform message-passing in learned latent graphs without explicit construction. In each GravNet layer, every node is mapped to a latent S -space where it learns intrinsic features. Each node’s S -space representation is then refined by aggregating information from its k -nearest neighbors using distance-weighted mean and max functions, and these aggregated features, along with the node’s original and S -space features, are updated via a fully-connected MLP.

The resulting features from each GravNet block are concatenated and passed through a single MLP to obtain F' hidden features for each strip. The new hidden geometry representation is truncated, masked, and sorted to align with the non-background STRIPIDs of the embedding module’s output z . The positional encoding module’s output g' is defined as

$$g' \in \mathbb{R}^{V \times F'} = f_{\text{PE}}(g; x), \quad (2)$$

and is added to the embedding module’s output z to serve as the input to the feature extraction module.

The feature extraction module f_{EXT} is composed of a Transformer encoder and a dense network for determining object condensation variables. The $V = 150$ length sequence of F' -dimensional tokens are passed through a background-masked self-attention mechanism. This masking allows every hit to attend to all others, capturing long-range relationships such as multi-sector clusters. The self-attention layer is followed by dropout and layer normalization. The resulting representation is then concatenated with the original sequence and forwarded through two fully-connected MLPs, after which another dropout is applied. A skip connection, combining the layer normalization output to the final dropout, gives the output of a single encoder block. After 4 consecutive encoder blocks, the sequence’s sorting is reversed to reflect the original ordering of the model’s inputs. The features of background hits are zeroed once more.

The hit representation is passed through a final dense network that determines a 2-dimensional latent space coordinate (x_c, y_c) and confidence measure β for each hit, such that:

$$y \in \mathbb{R}^{V \times 3} = f_{\text{EXT}}(z + g'). \quad (3)$$

5.2. Loss Function

The full network maps each ECal hit to a location in a 2-dimensional latent space and assigns it a confidence value between $\beta \in [0, 1]$. High values of β indicate a stronger condensation point. In the latent space, condensation points attract other hits belonging to the same cluster, and repel hits that belong to other clusters. To reinforce this behavior, Ref. [4] describes an attractive and repulsive potential loss \mathcal{L}_V . First, for each true cluster t , the hit with the highest β is named that cluster’s representative. The attractive loss is quadratic in the distance between a hit and its cluster’s representative, pulling it towards the condensation point. The repulsive loss is linear and repels hits from condensation points of other objects.

An additional loss term, the beta loss \mathcal{L}_β , helps tune the value of β for the hits. It is comprised of two components, the first being the ”coward loss” which rewards the network for maximizing the β of condensation points. The second component, the ”noise loss”, penalizes the model for assigning high β to noisy hits. The total object condensation loss to minimize is thus

$$\begin{aligned}\mathcal{L} &= \mathcal{L}_V + \mathcal{L}_\beta \\ &= \mathcal{L}_{\text{att}} + \mathcal{L}_{\text{rep}} + \mathcal{L}_{\text{cow}} + \mathcal{L}_{\text{nse}},\end{aligned}\tag{4}$$

where \mathcal{L}_{att} is the attractive loss, \mathcal{L}_{rep} is the repulsive loss, \mathcal{L}_{cow} is the coward loss and \mathcal{L}_{nse} is the noise loss.

Figure 6 shows how the training and validation losses evolve over the epochs. Note that dropout layers are disabled during validation, which explains the lower loss calculated on the validation set compared to the training set. We selected the final model parameters from epoch 77, as no further improvement was seen over the subsequent 10 epochs.

5.3. Inference

Clustering starts by first ordering all hits by their learned β . To create the first cluster, the highest β is chosen, and all hits within a distance $t_D = 0.28$ of it are grouped together. Then, the second cluster begins with the next highest β that is unclustered. We repeat this iteratively, forming clusters until the highest remaining β falls below the threshold $t_\beta = 0.5$. All remaining unclustered points are classified as noise.

In Figure 7, we compare the ECal clustering using COATJAVA and object condensation for a sample event’s detector response. Generated hits are mapped to locations in the OC latent space where the previously mentioned

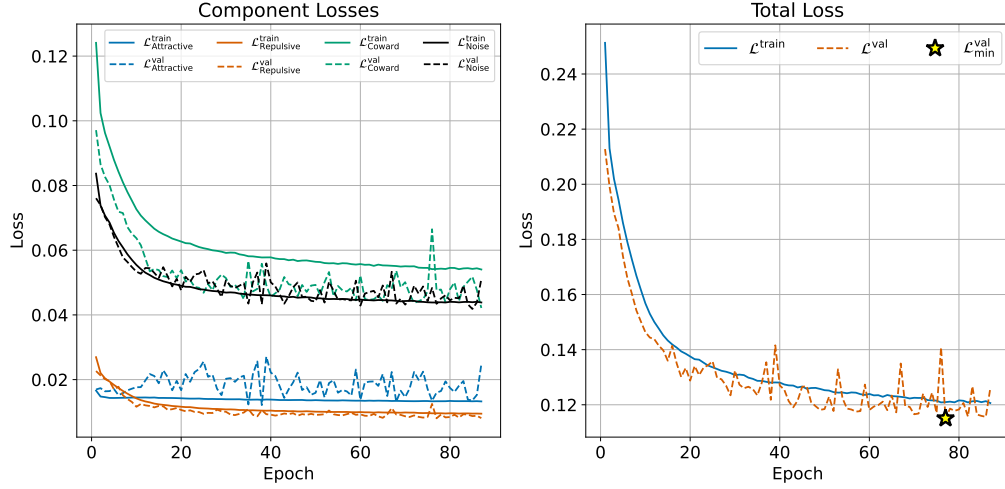


Figure 6: (Left) Components of the object condensation loss as a function of training epoch. (Right) Sum of the object condensation loss components as a function of training epoch. Dashed lines represent the validation loss.

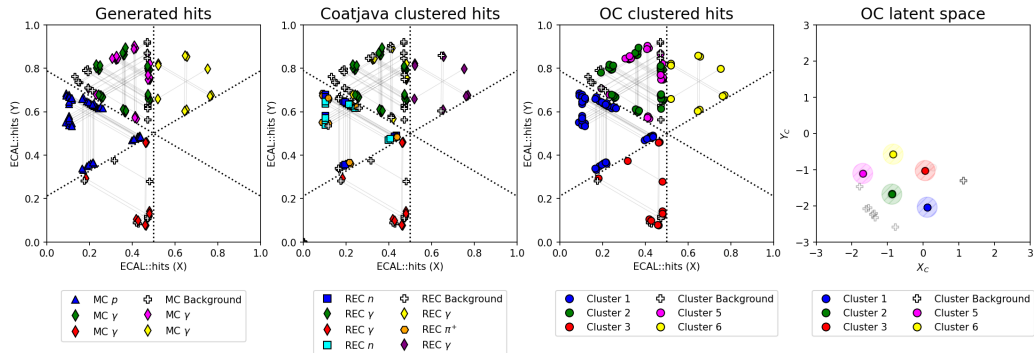


Figure 7: Leftmost plot shows simulated ECal detector response from multiple final state particles in a collision event. The center-left plot shows the clustering results from COAT-JAVA, and the center-right plot shows the clustering results from object condensation. The AI network maps each of the generated hits into the 2-d latent space shown and color-matched in the rightmost plot.

inference steps are taken to define OC clusters. In this example, COATJAVA incorrectly finds 2 additional neutron clusters, whereas object condensation does not.

5.4. Postprocessing

A postprocessing step transforms each group of strips into an ECal cluster object. These objects are sent through the rest of the COATJAVA reconstruction pipeline, allowing us to bypass the previous clustering algorithm.

Determining the cluster centroid is a two-step process. The first step collects N 3-way intersections for each cluster k . The second step uses those N 3-way intersections to calculate one cluster centroid for each cluster k . In more detail...

1. Loop over PCal, ECin, and Ecout strips

- For each strip j belonging to a cluster k , find its most energetic $\left(\sum_j E_j\right)$ 3-way intersection.
- A 3-way intersection is defined by the average (x, y, z) of the closest approach for strips uv , vw , and uw .
- The energy E_j for each strip is corrected to account for attenuation.

2. For each cluster k containing N 3-way intersections

- Only consider 3-way intersections in the sector with a 50%+ majority.
- Calculate the z-score z_i for each 3-way intersection (x, y, z) .
- Report the centroid's (x, y, z) as the weighted sum of the 3-way intersections, where $w_i = (1 + z_i^2)^{-1}$ to lessen the impact of distantly separated 3-way intersections.

Each cluster's energy deposited E and time of formation t are calculated using calibrated attenuation length factors. The AI-assisted ECal clusters are passed back into COATJAVA to yield a list of particles for the event.

6. Results

To compare the clustering results of COATJAVA and object condensation, we define a metric called "trustworthiness" for each reconstructed neutron. A neutron is considered trustworthy if it satisfies the following criteria:

1. There is a true generated neutron within $\Delta\theta \leq 4^\circ$ and $\Delta\phi \leq 4^\circ$.
2. There is no other reconstructed neutron within $\Delta\theta \leq 4^\circ$ and $\Delta\phi \leq 4^\circ$.

Assuming perfect reconstruction, all reconstructed neutrons would be considered trustworthy (apart from the situation where two true neutrons in an event have similar θ and ϕ , which at CLAS12 energies is very unlikely). Maximizing the percentage of trustworthy neutrons is critical for ensuring accurate neutron studies at CLAS12.

The trustworthiness of reconstructed neutrons was evaluated on the same simulated $e+p$ collision dataset described in Section 4. The results are shown in Figure 8 binned in neutron momentum and neutron scattering angle. In the forward detector, base COATJAVA reconstructs 86,121 neutrons, of which 7,735 (8.98%) are trustworthy. Object condensation reconstructs 29,292 neutrons, of which 8,979 (30.65%) are trustworthy. The AI-assisted clustering method developed triples the trustworthiness of reconstructed neutrons and greatly reduces the false neutron background.

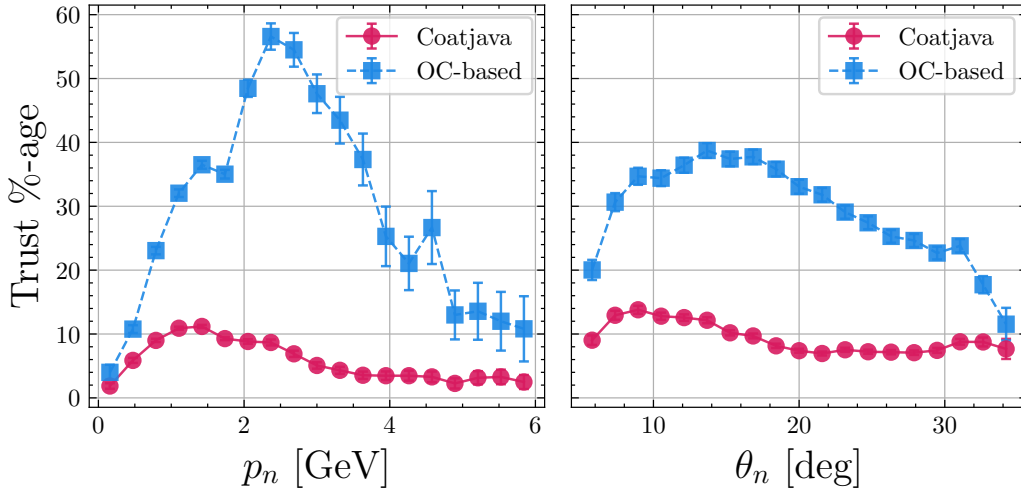


Figure 8: Trustworthiness of reconstructed neutrons as a function of momentum (left) and scattering angle (right).

In addition, the trustworthiness of reconstructed photons is shown in Figure 9 binned in photon momentum and photon scattering angle. Of the 180,417 forward detector photons reconstructed by base COATJAVA, 92,197 (51.10%) are trustworthy. Object condensation reconstructs 141,075 photons, of which 89,778 (63.64%) are trustworthy. While object condensation

does improve the trustworthiness of photons by +12%, the overall number of trustworthy photons is about 3% less. This is because photons, as opposed to neutrons, leave fewer total hits in the ECal. The object condensation framework can only assign one ECal hit to a true particle. As a consequence, cases where one strip is a part of two separate 3-way intersections (particles) are unresolvable. COATJAVA resolves this by duplicating strips, allowing the copies to belong to separate clusters. Recent advancements in computer vision — particularly multi-object classification models like Mask R-CNN [24] MaskFormer [14], YOLACT [25] and CondInst [26] — offer promising strategies to overcome these limitations.

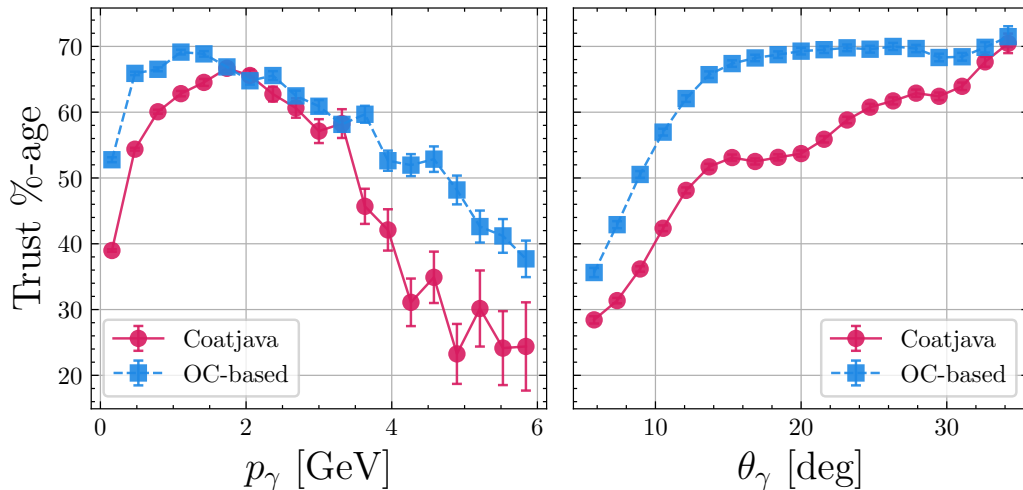


Figure 9: Trustworthiness of reconstructed photons as a function of momentum (left) and scattering angle (right).

7. Conclusion

This paper presents a novel AI approach to ECal hit clustering at CLAS12 using object condensation. Our model uses both GravNet layers for local message-passing and a Transformer encoder for long-range message-passing. The trained network was integrated into the existing CLAS12 reconstruction pipeline, where it was shown to outperform previous methods in producing reliable neutron and photon clusters.

To our knowledge, this study represents the first application of an AI-based clustering method to hodoscopic detectors. Our successful implemen-

tation widens the scope of clustering tasks that can be solved using AI. To improve the model, future work will be dedicated to exploring multi-object classification methods. We will also explore combining the clustering model with regression tasks such as reconstructing the cluster energy and position. The python project is available to view on GitLab [27].

CRedit authorship contribution statement

Gregory Matousek: Writing — original draft, Investigation, Formal analysis, Data curation, Funding acquisition, Methodology, Software, Visualization. **Anselm Vossen:** Writing — review & editing, Supervision, Funding acquisition, Project administration.

Acknowledgments

This material is based upon work supported by the U.S. Department of Energy, Office of Science, Office of Nuclear Physics under contract DE-SC0024505. This research was supported by the U.S. Department of Energy (DOE) and the National Science Foundation (NSF). We extend our gratitude to the DOE and NSF for their financial support, which made this work possible.

References

- [1] V. Burkert, L. Elouadrhiri, K. Adhikari, et al., The CLAS12 Spectrometer at Jefferson Laboratory, Nuclear Instruments and Methods in Physics Research Section A: Accelerators, Spectrometers, Detectors and Associated Equipment 959 (2020) 163419. doi:10.1016/j.nima.2020.163419.
- [2] S. R. Qasim, J. Kieseler, Y. Iiyama, et al., Learning representations of irregular particle-detector geometry with distance-weighted graph networks (Jul. 2019).
URL <http://arxiv.org/abs/1902.07987>
- [3] A. Vaswani, N. Shazeer, N. Parmar, et al., Attention Is All You Need (Aug. 2023). doi:10.48550/arXiv.1706.03762.
URL <http://arxiv.org/abs/1706.03762>

- [4] J. Kieseler, Object condensation: one-stage grid-free multi-object reconstruction in physics detectors, graph and image data (Sep. 2020). URL <http://arxiv.org/abs/2002.03605>
- [5] K. Lieret, G. DeZoort, D. Chatterjee, et al., High Pileup Particle Tracking with Object Condensation (Dec. 2023). doi:10.48550/arXiv.2312.03823. URL <http://arxiv.org/abs/2312.03823>
- [6] P. Calafiura, J. Chan, L. Delabrouille, et al., EggNet: An Evolving Graph-based Graph Attention Network for Particle Track Reconstruction (Jul. 2024). doi:10.48550/arXiv.2407.13925. URL <http://arxiv.org/abs/2407.13925>
- [7] HEPML Working Group, HEPML Living Review, <https://iml-wg.github.io/HEPML-LivingReview/>, accessed: 2025-03-03 (2023).
- [8] Y. Wang, Y. Sun, Z. Liu, et al., Dynamic Graph CNN for Learning on Point Clouds, ACM Trans. Graph. 38 (Oct. 2019). doi:10.1145/3326362. URL <https://doi.org/10.1145/3326362>
- [9] F. Wemmer, I. Haide, J. Eppelt, et al., Photon Reconstruction in the Belle II Calorimeter Using Graph Neural Networks, Computing and Software for Big Science 7 (2023) 13. doi:10.1007/s41781-023-00105-w.
- [10] S. Caillou, P. Calafiura, S. A. Farrell, et al., ATLAS ITk Track Reconstruction with a GNN-based pipeline, Tech. rep., CERN, Geneva (2022). URL <https://cds.cern.ch/record/2815578>
- [11] R. Liu, P. Calafiura, S. Farrell, et al., Hierarchical Graph Neural Networks for Particle Track Reconstruction (Mar. 2023). doi:10.48550/arXiv.2303.01640. URL <http://arxiv.org/abs/2303.01640>
- [12] A. Correia, F. I. Giasemis, N. Garroum, et al., Graph Neural Network-Based Track Finding in the LHCb Vertex Detector (Dec. 2024). doi:10.48550/arXiv.2407.12119. URL <http://arxiv.org/abs/2407.12119>

- [13] S. V. Stroud, P. Duckett, M. Hart, et al., Transformers for Charged Particle Track Reconstruction in High Energy Physics (Nov. 2024). doi:10.48550/arXiv.2411.07149.
URL <http://arxiv.org/abs/2411.07149>
- [14] B. Cheng, A. G. Schwing, A. Kirillov, Per-Pixel Classification is Not All You Need for Semantic Segmentation (Oct. 2021). doi:10.48550/arXiv.2107.06278.
URL <http://arxiv.org/abs/2107.06278>
- [15] S. R. Qasim, K. Long, J. Kieseler, et al., Multi-particle reconstruction in the High Granularity Calorimeter using object condensation and graph neural networks (Jun. 2021). doi:10.48550/arXiv.2106.01832.
URL <http://arxiv.org/abs/2106.01832>
- [16] G. Asryan, S. Chandavar, T. Chetry, et al., The CLAS12 forward electromagnetic calorimeter, Nuclear Instruments and Methods in Physics Research Section A: Accelerators, Spectrometers, Detectors and Associated Equipment 959 (2020) 163425. doi:10.1016/j.nima.2020.163425.
- [17] C. M. S. Collaboration, Particle-flow reconstruction and global event description with the CMS detector, Journal of Instrumentation 12 (2017) P10003–P10003. doi:10.1088/1748-0221/12/10/P10003.
- [18] Electron and photon reconstruction and identification in ATLAS: expected performance at high energy and results at 900 GeV, Tech. rep., CERN, Geneva (2010).
URL <https://cds.cern.ch/record/1273197>
- [19] A. Collaboration, Performance of the ALICE Electromagnetic Calorimeter, Journal of Instrumentation 18 (2023) P08007. doi:10.1088/1748-0221/18/08/P08007.
- [20] D. Allan, C. Andreopoulos, C. Angelsen, et al., The Electromagnetic Calorimeter for the T2K Near Detector ND280, Journal of Instrumentation 8 (2013) P10019–P10019. doi:10.1088/1748-0221/8/10/P10019.
- [21] F. Collaboration, W. B. Atwood, The Large Area Telescope on the Fermi Gamma-ray Space Telescope Mission, The Astrophysical Journal 697 (2009) 1071–1102. doi:10.1088/0004-637X/697/2/1071.

- [22] G. A. Fiorentini, The MINERvA detector, AIP Conference Proceedings 1663 (2015) 020002. doi:10.1063/1.4919462.
URL <https://doi.org/10.1063/1.4919462>
- [23] J. Lab, clas12-mcgen: Monte Carlo Event Generators for CLAS12, accessed: 2025-03-03 (2024).
URL <https://github.com/JeffersonLab/clas12-mcgen>
- [24] K. He, G. Gkioxari, P. Dollár, R. Girshick, Mask r-cnn (arXiv:1703.06870), arXiv:1703.06870 [cs] (Jan. 2018). doi:10.48550/arXiv.1703.06870.
URL <http://arxiv.org/abs/1703.06870>
- [25] D. Bolya, C. Zhou, F. Xiao, Y. J. Lee, Yolact: Real-time instance segmentation (arXiv:1904.02689), arXiv:1904.02689 [cs] (Oct. 2019). doi:10.48550/arXiv.1904.02689.
URL <http://arxiv.org/abs/1904.02689>
- [26] Z. Tian, C. Shen, H. Chen, Conditional convolutions for instance segmentation (arXiv:2003.05664), arXiv:2003.05664 [cs] (Jul. 2020). doi:10.48550/arXiv.2003.05664.
URL <http://arxiv.org/abs/2003.05664>
- [27] Gregory Matousek, Comet, <https://code.jlab.org/gmat/comet>, accessed: 2025-02-26 (2025).